DOI 10.1007/s11106-020-00125-w
Powder Metallurgy and Metal Ceramics, Vol. 58, Nos. 11-12, March, 2020 (Russian Original Vol. 58, Nos. 11-12, Nov.-Dec., 2019)

COMPOSITE MATERIALS

EFFECT OF VACUUM HOT PRESSING TEMPERATURE ON THE MECHANICAL AND TRIBOLOGICAL PROPERTIES OF THE Fe–Cu–Ni–Sn–VN COMPOSITES

V.A. Mechnik,[1,4] N.A. Bondarenko,[1] V.M. Kolodnitskyi,[1] V.I. Zakiev,[2] I.M. Zakiev,[2] S.R. Ignatovich,[2] S.N. Dub,[1] and N.O. Kuzin[3]

UDC 620.22–621.921.34

The mechanical (hardness and elastic modulus) and tribological (friction force and wear rate) properties of the Fe–Cu–Ni–Sn–VN composites produced by cold pressing and subsequent vacuum hot pressing at different temperatures are studied. The starting iron, copper, nickel, and tin powders have 5–50 μm particles and the vanadium nitride powder has 0.1–0.7 μm particles. When vacuum hot pressing temperature rises from 800 to 1000°C, the hardness increases from 3.75 to 5.37 GPa and the elastic modulus decreases from 176 to 125 GPa. As a result, the friction force reduces from 115 to 80 mN and the wear rate from 1.93 · 10^{-5} to 0.45 · 10^{-5} $mm^3 \cdot N^{-1} \cdot m^{-1}$. The factors promoting improvement of the mechanical and tribological properties of the sintered composites are discussed. In particular, the main factor improving the mechanical properties is that the grains are refined from 5–50 μm to 20–400 nm through the $\alpha \rightarrow \gamma \rightarrow \alpha$ transformation when VN dissolves in α-Fe. In this case, the composite consists of a supersaturated solid solution of nitrogen and vanadium in α-iron, intermetallic Cu_9NiSn_3, and primary and secondary particulate vanadium nitride phases. A relationship between the structure and mechanical and tribological properties is established. The H/E and H^3/E^2 parameters that describe the elastic strain resistance and plastic strain resistance correlate with the wear resistance. The sintered composites are regarded as promising materials for developing a new generation of diamond-containing composites for stone processing industry.

Keywords: *composite, sintering temperature, structure, particle size, hardness, elastic modulus, friction force, wear.*

INTRODUCTION

Diamond-containing composites (DCCs) with metallic matrices including iron, copper, nickel, and tin are thoroughly examined since they are capable of imparting the required mechanical and tribological properties to the resultant articles [1–6] and the starting components are relatively inexpensive. The composites find application as

[1]Bakul Institute for Superhard Materials, National Academy of Sciences of Ukraine, Kyiv, Ukraine. [2]National Aviation University, Kyiv, Ukraine. [3]Dnipro National University of Rail Transport, Lviv Branch, Lviv, Ukraine.

[4]To whom correspondence should be addressed; e-mail: vlad.me4nik@ukr.net.

Translated from Poroshkova Metallurgiya, Vol. 58, Nos. 11–12 (530), pp. 73–90, 2019. Original article submitted October 22, 2018.

cutting wheels, wire saws, crowns, and grinding and polishing tools for the stone processing industry [7, 8]. Stone-working tools perform at high loads [9], stresses [10, 11], and temperatures [12–15]. This causes intensive wear of the metallic matrix [16–18] and imposes high requirements for the mechanical and tribological properties of DCCs. The application of such DCCs is to be extended and their mechanical and service properties are to be improved.

The physical factors improving the wear resistance of DCCs have been under active research in recent decay by many teams of scientists, making their contribution to the expansion of knowledge in materials science and solid state physics. These research efforts focus on the phase diagrams and structural characteristics of the composites in relation to the sintering methods and conditions, in line with the well-known 'composition–structure–particle size–property' dependence [19–21].

The techniques used to examine the structure and properties of DCCs with a coarse-grained Fe–Cu–Ni–Sn matrix produced by powder metallurgy methods are reviewed in [22]. Modern physical analysis methods were employed to study the elemental and phase composition, structure, and strength of DCCs with a Fe–Cu–Ni–Sn matrix containing vanadium nitride (VN) as a function of sintering parameters [23]. The cited paper showed that the mechanical properties of DCCs could be controlled through directional changes in the structure and phase composition.

The research area associated with the production of nanostructured materials consisting of at least two phases with a nanocrystalline and (or) amorphous structure is being developed actively [24–29]. The reason is that the mechanical properties of nanocomposite materials substantially differ from those of the same coarse-grained materials [30–32]. High hardness and wear resistance are noticeable among the unconventional properties of nanocrystalline materials. The hardness of nanocrystalline Cu–Fe materials is known to be two to seven times higher than that of the same coarse-grained materials [33]. According to [34], the microhardness of the Cu–Fe nanocomposite increases through the formation of interfaces with greater dislocation density since Cu and Fe have different (fcc and bcc) lattices. Contrastingly to the conventional concept about a direct relationship between the strength and elastic modulus for coarse-grained materials, the elastic modulus (E) and shear modulus (G) of grains approaching the nanosized range abruptly decrease while their strength increases [35]. These effects are manifested when the average grain size is no more than 100 nm and are most prominent when the grains are smaller than 10 nm [36]. The wear resistance of nanostructured materials is much greater than that of coarse-grained ones. The wear rate decreases from 1330 to 7.9 $\mu m^3/\mu m$ with the nickel grain size reducing from 10 μm to 10 nm [37]. Hence, the grains must be refined to the extent possible in producing the composites to substantially improve their wear resistance.

The influence of nanocrystalline state on the mechanical properties of the Fe–Cu–Ni–Sn matrix has been poorly studied and is hardly discussed in the literature. The paper [38] shows that addition of 3 wt.% nanosized VN powder to the 51Fe–32Cu–9Ni–8Sn mixture with 2,000–50,000 nm grains allows cold pressing at 500 MPa and subsequent vacuum hot pressing at 1000°C to be used to form 20–400 nm grains. This increases the nanohardness from 4.56 to 5.37 GPa, decreases the elastic modulus from 191 to 125 GPa and the friction force from 76 to 50 mN, and improves the wear resistance of the composite [39]. The application of materials with nanocrystalline matrices requires the hot pressing temperature range to be extended from 800 to 1000°C and its effect on the mechanical properties of DCCs to be examined.

Metallic matrices for DCCs for tribological applications must show low abrasive wear, high fatigue strength, and excellent elastic and plastic properties. According to [40], low abrasive wear is commonly associated with high hardness, which has been repeatedly observed for DCCs [7, 8, 21]. Hence, assessment of tribological characteristics of DCCs should consider that the matrix hardness is connected with elastic and plastic properties. Most bulk materials with high hardness have high elastic modulus E and are thus brittle. However, the wear resistance of many materials, including nanocomposites, and their elastic strain resistance were found to be proportional to the H/E ratio [41, 42].

To assess the plastic strain resistance, the H^3/E^2 parameter is used [43]. The paper [44] notes that the H^3/E^2 ratio also determines the friction coefficient and wear resistance. This means that the composite must possess high hardness and low elastic modulus to increase the elastic strain resistance and decrease the plastic strain. To optimize

and predict the tribological properties of DCCs, one should bear in mind that their wear resistance is influenced by the tool working surface [45].

An important feature of the Fe–Cu–Ni–Sn–VN composites is that the supersaturated solid solution of nitrogen and vanadium in α-iron decomposes when cooled down. In the process, the ferritic grains are refined and the thermal stability of nanosized (≈5–10 nm) nitride precipitates increases, imparting strength to the composites [38]. This method is economical as there is no need to use expensive nanopowders to improve the wear resistance of the composites.

There has been no experimental determination of nanohardness H, elastic modulus E, or H/E and H^3/E^2 ratios, nor has there been any study to ascertain how these parameters relate to the structure and tribological characteristics of the composites. These properties are studied individually in the literature; moreover, they belong to different materials and structural states. This greatly complicates analysis of common or distinctive features of DCCs and features peculiar to their production and application.

The objective is to examine the mechanical and tribological characteristics of the Fe–Cu–Ni–Sn–VN composites produced by cold pressing and subsequent vacuum hot pressing at 800, 900, and 1000°C and at 30 MPa.

EXPERIMENTAL PROCEDURE

Starting Materials and Sintering Method. To make samples 10 mm in diameter and 8 mm in thickness employing pressing at room temperature followed by vacuum hot pressing, we used a mixture of 49.47Fe–31.04Cu–8.73Ni–7.76Sn–3VN powders (composition is in wt.% here and further in the text). The powder mixture was prepared from PZhM2 iron, PMS-1 copper, PNE nickel, PO-1 tin (Powder Metallurgy Plant, Zaporizhzhia, Ukraine) with grain sizes from 5 to 50 μm, and vanadium nitride (CAS RN 24646-85-3, ONYXMET, Poland) with grain sizes from 0.1 to 0.7 μm. The powders were dry mixed in a drum with an offset rotation axis for 8 h. The weighed portions were compacted at room temperature in steel dies at 500 MPa using a hydraulic press. The compacts were then sintered by vacuum hot pressing in graphite dies at 800°C (sample 1), 900°C (sample 2), and 1000°C (sample 3) for 12 min at a final pressure of 30 MPa [46]. The samples were heated to isostatic holding temperature at a constant rate of 200°C/min. For reference, sample 4 with a diameter of 10 mm and a thickness of 8 mm was compacted at room temperature from the 51Fe–32Cu–9Ni–8Sn powder mixture. The average particle size of components in this mixture was 5–50 μm as well. Sample 4 was sintered in a steel die at 800°C for 60 min and then additionally subjected to hot pressing at 160 MPa [4].

Microstructural and Micromechanical Characteristics. The crystallite morphology and size distribution in the vanadium nitride powder and starting mixtures were examined on images taken with a REM-106I scanning electron microscope (Sumy, Ukraine) with an acceleration potential of 30 kV. No less than 20 images were taken for each sample. Electron microscopy analysis of thin foils from sintered samples was carried out to produce diffraction patterns with a TEM-125 transmission electron microscope (Sumy, Ukraine) with an acceleration potential of 125 kV and 0.18 nm resolution. The interplanar spacing was estimated from selected-area electron diffraction patterns with an internal MgO standard. The quantitative phase composition was calculated using full-profile analysis with the MAUD software. The thin foils from sintered samples for microstructural analysis were obtained by electrolytic polishing in an $HClO_4$ + 30% HNO_3 + H_2O solution.

X-ray diffraction patterns for the samples were taken with a DRON 4.13C diffractometer in copper anode radiation in the Bragg–Brentano geometry at $20° \le 2\theta \le 80°$. The standard procedure with the X-powder software was employed for X-ray diffraction [47]. The diffraction spectra with refined spacing d_i for the phase lattices and relative reflection intensities I_i of the phases were identified by comparison with the reference spectra using the ASTM–ICPDS data files [48].

The chemical composition was calculated with ZAF corrections by the Magelanes 3.1 software. The errors of determination were as follows: ~0.01 wt.% for heavy elements and ~1 wt.% for light ones.

Micromechanical and Tribological Tests. To assess the micromechanical properties (nanohardness H and elastic modulus E), the samples were tested with a Berkovich indenter using a Nano Indenter II system (MTS

Systems Corporation, USA) at a load of 5 mN. The load was increased constantly and reached 0.2 mN/sec. The hardness and elastic modulus were found from the indenter unloading curve with Oliver and Pharr's method [49].

Tribological tests of the sintered samples were performed at an ambient temperature of 25°C and a relative humidity of ≈50% using a 'pin (indenter)–disk (sample)' scratch tester [39]. The samples were preliminary polished with SiC with particles up to 5 μm in size and an oxide suspension with colloidal silicon dioxide particles 100 nm in size. The tests were performed with a conical diamond indenter with a 50 μm radius at the tip rotating (115 revolutions) over the samples under a load of 4.91 N at a sliding speed of 20 μm/sec. The wear weight loss V (volume of friction paths) was quantitatively measured with a Micron-Alpha interference 3D surface analyzer [50], recording surface irregularities with nanometer accuracy. The data were then converted to the wear rate. It was determined as $I = V/(P_N L \cdot n)$, where V is the sample's volume loss, μm^3; P_N is normal load, N; $L = \pi D$ is the path length, μm; n is the number of revolutions; and D is the friction path diameter. The tests comply with international standards ASTM G99-959, DIN50324, and ISO 20808.

To ascertain the reliability of the data obtained and interpret the wear mechanisms, additional scratch tests of the sintered samples were performed with a Vickers indenter under a load of 4.91 N at a sliding speed of 20 μm/sec. The scratch length was 5 mm.

EXPERIMENTAL RESULTS AND DISCUSSION

Micromechanical Properties. Table 1 summarizes nanohardness H, elastic modulus E, elastic strain resistance H/E, and plastic strain resistance H^3/E^2 determined for the sintered samples with grains of different size. The H, E, and H/E parameters for samples 1 and 2 sintered at 800 and 900°C hardly differ. These samples have the same structure and consist of a solid solution of Fe–Cu (grain size $d_{av} \approx$ 5,000–25,000 nm) and Cu_9NiSn_3 and $Cu_{40.5}Sn_{11}$ compounds [7]. The hardness of sample 3 sintered at a higher temperature (1000°C) increases from 3.75 to 5.37 GPa and elastic modulus decreases to 125 GPa. An abrupt increase in H/E (from 0.021 to 0.043) and H^3/E^2 (from 1.70 to 9.91 GPa) is observed. The H, H/E, and H^3/E^2 parameters increase and parameter E decreases in sample 3 (versus samples 1 and 2) because the grains are refined and there is no residual (unreacted) low-hardness austenite (fcc phase). The average grain size of basic components in sample 3 is 20–400 nm. Sample 3 consists of a supersaturated solid solution of nitrogen and vanadium in α-iron and a mixture of nanosized VN and VO_2 phases [38].

Therefore, the main factors that improve the mechanical properties of sample 3 compared to samples 1 and 2 are that there is a bcc phase and grains are refined. The behavior of hardness agrees with the Hall–Petch relationship, associating the increase in hardness with grain refinement. Such H and H/E values at low elastic moduli (E ~114 GPa) were also obtained in the examination of multicomponent nanocrystalline titanium alloys [51]. Noteworthy is that the paper [34] found that the elastic moduli of Cu and Ni became 10–15% lower.

The lowest H (2.68 GPa), H/E (0.013), and H^3/E^2 (0.49 GPa) parameters were shown by sample 4 (Table 1) produced from the 51Fe–32Cu–9Ni–8Sn mixture by cold pressing followed by sintering with additional pressing. The mechanical properties deteriorated because sample 4 was coarse-grained. The grain sizes were assessed as 5,000–50,000 nm in [4].

TABLE 1. Mechanical Properties of Sintered Samples

Sample	Temperature, °C	Grain size, nm	Nanohardness H, GPa	Elastic modulus E, GPa	H/E	H^3/E^2, MPa
1	800	5,000–20,000	3.75	176	0.021	1.70
2	900	5,000–25,000	3.77	177	0.021	1.71
3	1000	20–400	5.37	125	0.043	9.91
4	800	2,000–50,000	2.68	199	0.013	0.49

[*] The nanohardness of iron-containing regions was determined because of relatively small sizes of VN grains (5–50 nm [38]).

The data indicate that the mechanical properties of the sintered samples are determined by their structure, composition, and sintering conditions. Samples 1 and 2 are coarse-grained ($d \approx 5{,}000$–$25{,}000$ nm) and are characterized by relatively low H (≈3.56–3.77 GPa), H/E (≈0.020–0.021), and H^3/E^2 (≈1.47–1.71 MPa) and relatively high elastic modulus ($E \approx 175$–177 GPa). The grain refinement from 5,000–20,000 nm to 20–400 nm in the production of sample 3 (versus samples 1 and 2) is accompanied by a decrease in the elastic moduli from 176 to 125 GPa and an increase in the nanohardness from 3.75 to 5.57 GPa. These patterns increase H/E by two times and H^3/E^2 by 5.8 times. The results suggest that sample 3 should have high wear resistance (unlike samples 1 and 2). A number of papers reported that the mechanical properties of nanocomposite materials improved as compared to the same coarse-grained materials. The paper [33] showed that hardness of the nanosized Cu–Fe composite was two to seven times higher than that of the coarse-grained composites. The paper [52] indicated that the nanosized Ti–24Nb–4Zn–7.9Sn alloy with a bcc lattice had high hardness and low elastic modulus. A 10–15% decrease in the elastic moduli of Cu and Ni was found in [34].

Therefore, the mechanical properties of sintered composites improve with grain refinement. In the process, the elastic strain resistance and plastic strain resistance increase in the composites with higher hardness and lower elastic modulus. The most interesting finding is that fine-grained structures might have greater wear resistance than coarse-grained ones.

Tribological Properties. Figure 1 shows how the friction force F_{fr} changes with time in rotational movement of a diamond indenter over the surface of sintered samples. As is seen, F_{fr} depends on the composition, temperature, and sintering method. Hence, average F_{fr} for sample 1 produced at 800°C is ≈115 mN (Fig. 1*a*), which is somewhat lower than $F_{fr} \approx 100$ mN for sample 2 (Fig. 1*b*) sintered at 900°C. The great difference in F_{fr} for these samples is due to the coarse-grained structure ($d \approx 5{,}000$–$25{,}000$ nm). The friction force significantly decreases (≈80 mN) for sample 3 (Fig. 1*c*) sintered at 1000°C, contrastingly to samples 1 and 2 sintered at lower temperatures (800 and 900°C). The friction force decreases and remains stable because the grains are refined from 5,000–20,000 nm to 20–400 nm and the mechanical properties are improved (Table 1).

The highest F_{fr}, about 125 nm, was observed for sample 4 (Fig. 1*d*) sintered at 800°C and then subjected to additional hot pressing. The coarse-grained structure is the physical factor behind the increase in friction force and, hence, friction coefficient. In this case, the grain sizes are assessed at about 2,000–50,000 nm in accordance with [4].

An important finding is that the H, H/E, and H^3/E^2 parameters increase when the friction force of sample 3 decreases (Table 1).

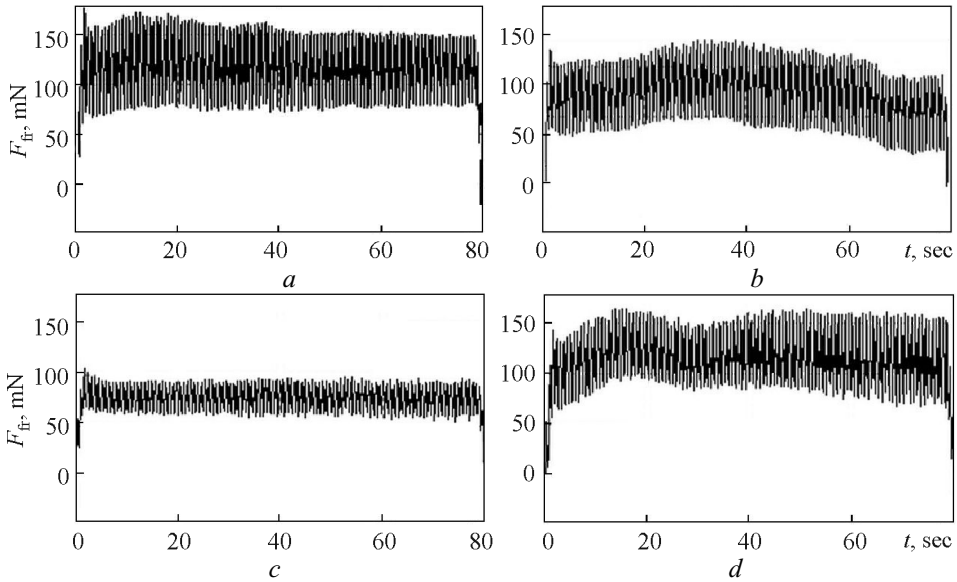

Fig. 1. Friction force F_{fr} versus time for samples 1 (*a*), 2 (*b*), 3 (*c*), and 4 (*d*)

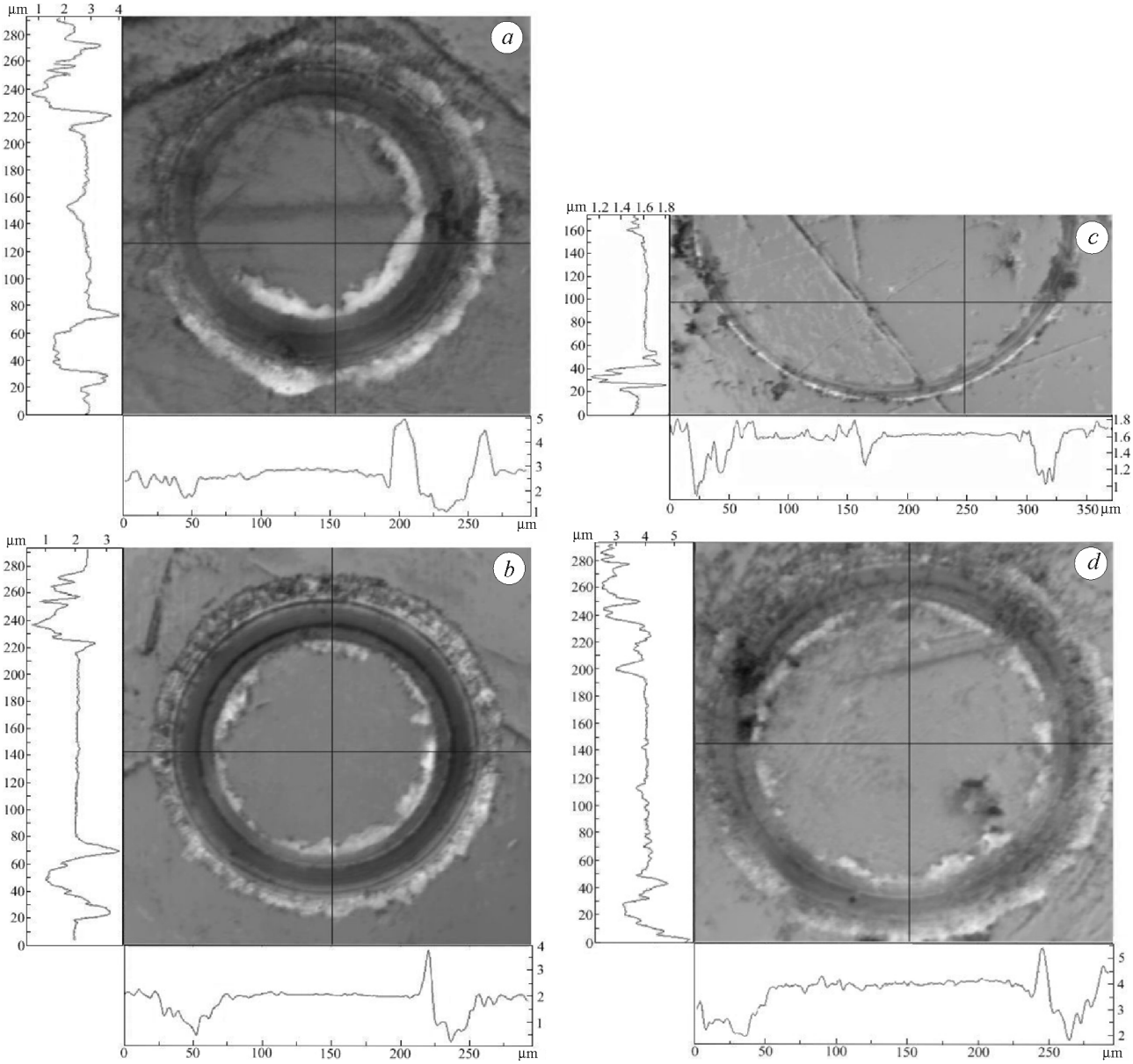

Fig. 2. 2D topographies of friction paths: *a*, *b*, *c*, and *d*) samples 1, 2, 3, and 4, respectively

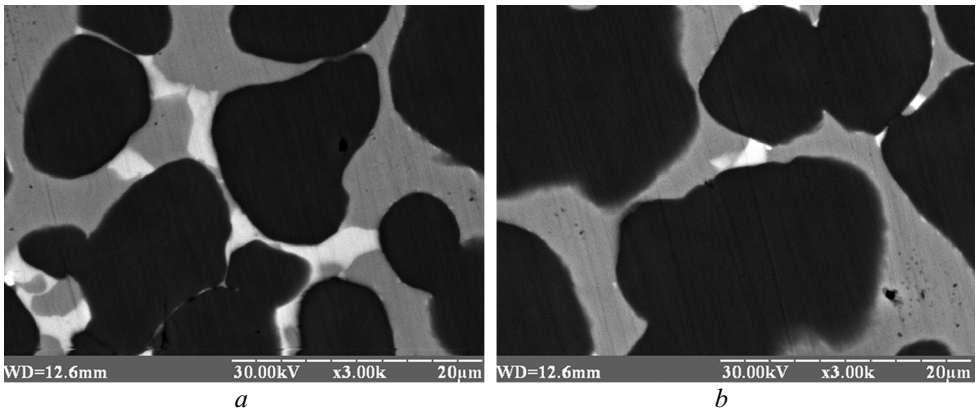

a *b*

Fig. 3. Structure of samples 1 (*a*) and 2 (*b*) sintered from the 51Fe–32Cu–9Ni–8Sn mixture at $T = 800$ (*a*) and 900°C (*b*)

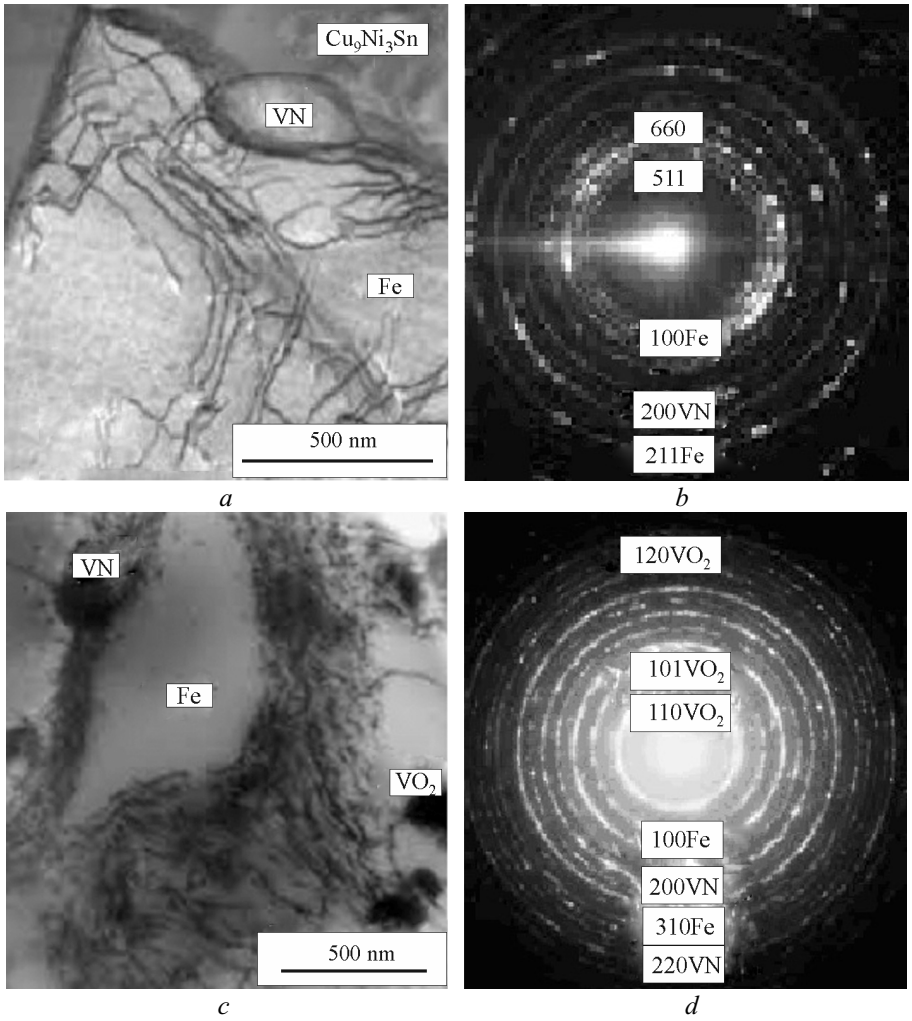

Fig. 4. Structures (*a, c*) and associated electron diffraction patterns (*b*, *d*) for the 49.47Fe–31.04Cu–8.73Ni–7.76Sn–3VN composite sintered at 1000°C

Figure 2 illustrates how the topography of friction paths (friction path width and depth) changes. With increasing sintering time, the wear path width and depth decrease for all samples.

After wear tests, sample 2 sintered at 900°C shows lower wear rate ($1.87 \cdot 10^{-5}$ mm$^3 \cdot$ N$^{-1} \cdot$ m^{-1}) than sample 1 ($1.93 \cdot 10^{-5}$ mm$^3 \cdot$ N$^{-1} \cdot$ m^{-1}) sintered at a lower temperature (800°C) (Table 2). When vacuum hot pressing temperature further increases from 900 to 1000°C, the wear rate of sample 3 decreases from $1.87 \cdot 10^{-5}$ to $0.45 \times \times 10^{-5}$ mm$^3 \cdot$ N$^{-1} \cdot$ m^{-1} compared to sample 2. The wear resistance of sample 3 increases versus samples 1 and 2 because the ferritic grains are refined from 5,000–25,000 nm to 20–400 nm and, moreover, nanosized VN and VO_2 phases are present.

Noteworthy is that a minimum wear rate of $0.45 \cdot 10^{-5}$ mm$^3 \cdot$ N$^{-1} \cdot$ m^{-1} was reached for sample 3, which is characterized by the highest H, H/E, and H^3/E^2 parameters equal to 5.37 GPa, 0.043, and 9.91 MPa, respectively, and the lowest elastic modulus equal to 125 GPa (Table 1).

The images in Fig. 3 (scanning electron microscopy) and Fig. 4 (transmission electron microscopy) directly indicate that the microstructure influences the mechanical and tribological properties of the sintered composites. Sample 1 (Fig. 3*a*) and sample 2 (Fig. 3*b*) sintered at 800 and 900°C from the mixture without vanadium nitride have a coarse structure with 5–15 μm grains. The fine-grained α-Fe ferrite (grain sizes varying from 20 to 400 nm) and intermetallic Cu_9NiSn_3 phases ≤400 nm in size (Fig. 4*a*) form in sample 3 produced from the mixture containing vanadium nitride. The sizes of vanadium nitride (VN) and vanadium oxide (VO_2) particles range from 5

to 100 nm (Fig. 4*a*, *c*). The 50 nm and larger VN particles are primary powder particles. The particles within 10 nm in size are secondary VN particles that precipitated in the decomposition of the supersaturated solid solution of nitrogen and vanadium in α-iron. The nitrides are located at grain boundaries and in the bulk, primarily on dislocations. The electron diffraction patterns show ring reflections from (110), (211), (200), and (310) planes of bcc α-Fe, (511) and (660) planes of Cu_9NiSn_3, (220) and (200) planes of VN, and (120), (101), and (110) planes of VO_2 (Fig. 4*b*, *d*). The abrupt decrease in the grain size in the sample with vanadium nitride (compared to the sample without VN) is accompanied by an increase in hardness H from 2.68 to 5.37 GPa, elastic strain resistance H/E from 0.013 to 0.043, plastic strain resistance H^3/E^2 from 0.49 to 9.91 MPa (Table 1), and wear resistance by four times (Table 2). Therefore, the initial microstructure of the composites substantially influenced their mechanical and tribological properties in wear.

Improvement in the tribological properties through increase in hardness and some decrease in elastic modulus was also reported in [53, 54].

The maximum wear rate, $2.46 \cdot 10^{-5}$ mm$^3 \cdot$ N$^{-1} \cdot$ m^{-1}, was recorded for sample 4 with lowest H, H/E, and H^3/E^2 equal to 2.68 GPa, 0.013, and 0.49 MPa and, accordingly, with highest elastic modulus equal to 199 GPa (Table 1). The tribological properties of this sample deteriorated because of its coarse-grained structure. The grain sizes are approximately 2,000–50,000 nm (Fig. 5).

The data obtained indicate that the wear resistance of the composites improves with decreasing grain size and increasing H, H/E, and H^3/E^2. To ascertain the reliability of the results, the sintered samples were subjected to scratch tests with a Vickers indenter under a load of 4.91 N and a sliding speed of 20 μm/sec. Figure 6 presents dependences of the friction force F_{fr} on the path left by the indenter on the sintered samples. The initial running-in path, when the friction force and thus the friction coefficient levelled off, was sufficiently short for all samples (≈30 μm). The friction force decreased with higher vacuum hot pressing temperature. The friction force reduced for sample 3 (Fig. 6*c*) produced by vacuum hot pressing at 1000°C as compared to samples 1 and 2 (Fig. 6*a*, *b*) sintered at lower temperatures (800 and 900°C). This is due to grain refinement from 5,000–25,000 nm to 20–400 nm and improvement in the mechanical properties (Table 1). The lower friction force for sample 3 compared with samples

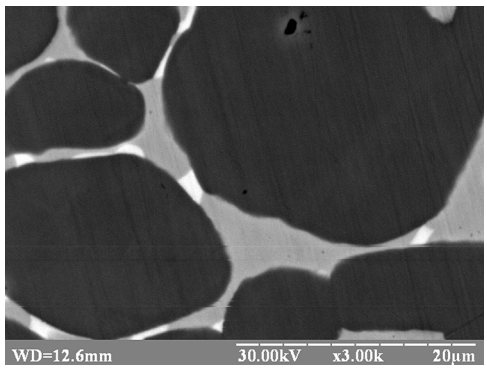

Fig. 5. Structure of sample 4 produced from the 51Fe–32Cu–9Ni–8Sn mixture by pressing at room temperature and sintering at 800°C with additional hot pressing at 160 MPa

TABLE 2. Tribological Properties of Sintered Samples

Sample	Temperature, °C	Grain size d, nm	Friction path diameter D, μm	Friction path volume V, 10^{-3} mm^3	Wear rate I, 10^{-5} mm$^3 \cdot$ N$^{-1} \cdot$ m^{-1}
1	800	5,000–20,000	245	8.39	1.93
2	900	5,000–25,000	195	6.47	1.87
3	1000	20–400	320	2.56	0.45
4	800	2,000–50,000	185	8.08	2.46

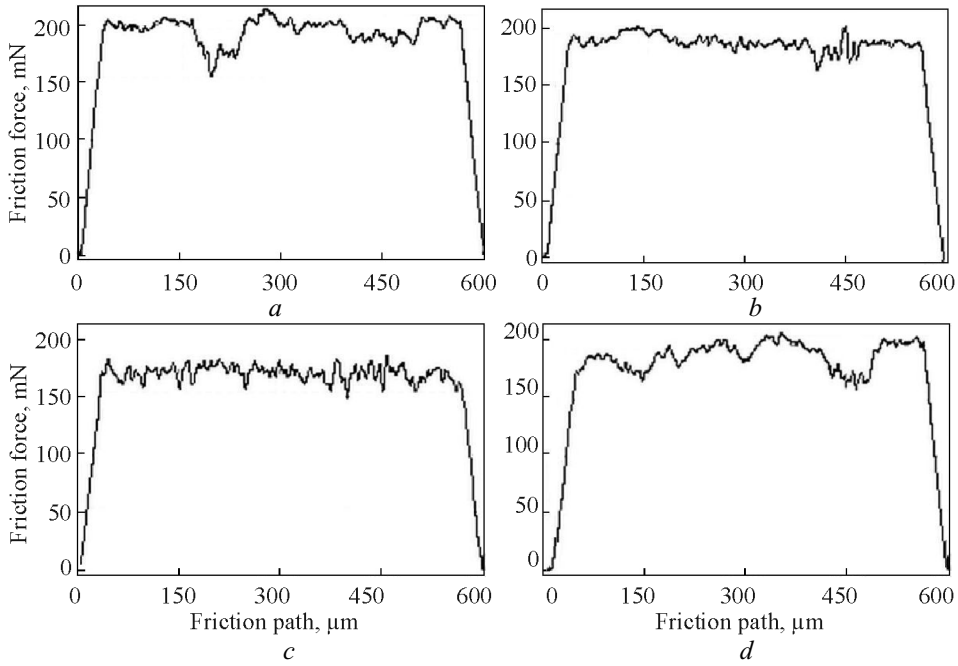

Fig. 6. Friction force versus friction path left by the Vickers indenter on samples 1 (*a*), 2 (*b*), 3 (*c*), and 4 (*d*)

1 and 2 is associated with its nanosized structure and the presence of VN and VO_2 phases (5–100 nm) (Fig. 4). The highest F_{fr} values were recorded for sample 4 (Fig. 6*d*), which is due to coarse-grained structure. The grain sizes are approximately 2,000–50,000 nm (Fig. 5).

A typical finding is that the decrease in the friction force for sample 3 is accompanied by an increase in H, H/E, and H^3/E^2 (Table 1).

Figure 7 shows 3D topographies of the friction paths. Their analysis indicates that the wear path volume substantially depends on sintering temperature.

The wear rate of sample 1 sintered at 800°C is $1.76 \cdot 10^{-5}$ mm$^3 \cdot$ N$^{-1} \cdot$ m^{-1} (Table 3), which is comparable with its wear rate determined in pin-on-disk test ($1.93 \cdot 10^{-5}$ mm$^3 \cdot$ N$^{-1} \cdot$ m^{-1}) (Table 2). The wear rate of sample 2 sintered at 900°C was somewhat lower. The wear rate of sample 3 sintered at 1000°C was minimum: $0.71 \times$ $\times 10^{-5}$ mm$^3 \cdot$ N$^{-1} \cdot$ m^{-1}. The lower wear rate of sample 3 compared to samples 1 and 2 results from the same patterns as discussed above for the friction force and wear rate in tests of sintered samples by a rotating diamond indenter (Figs. 1 and 2). The wear rates determined by testing of sintered samples 1–4 (Table 3) correlate with hardness H, elastic strain resistance H/E, and plastic strain resistance H^3/E^2 (Table 1).

The minimum wear rate, $2.58 \cdot 10^{-5}$ mm$^3 \cdot$ N$^{-1} \cdot$ m^{-1}, was recorded for sample 4 with lowest H, H/E, and H^3/E^2 equal to 2.68 GPa, 0.013, and 0.49 MPa and highest elastic modulus equal to 199 GPa (Table 1). The tribological properties of this sample are due to its coarse-grained structure (d_{av} = 2,000–50,000 nm). Comparison of the results

TABLE 3. Tribological Properties of Sintered Samples

Sample	Temperature, °C	Grain size d, nm	Friction path volume V, 10^{-7} mm^3	Wear rate I, 10^{-5} mm$^3 \cdot$ N$^{-1} \cdot$ m^{-1}
1	800	5,000–10,000	4.32	1.76
2	900	5,000–10,000	3.95	1.61
3	1000	20–400	1.73	0.71
4	800	2,000–50,000	6.33	2.58

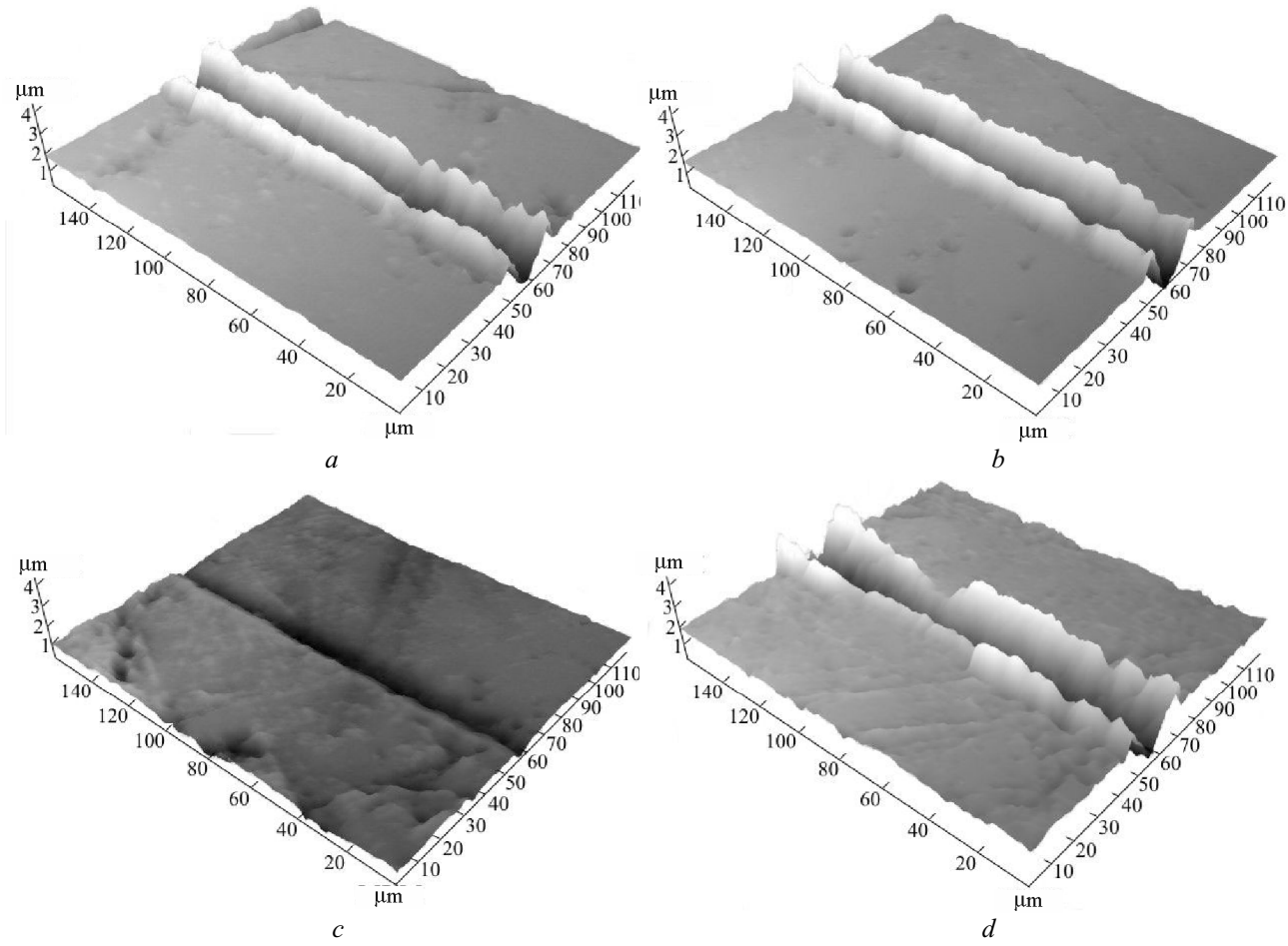

Fig. 7. 3D topographies of friction paths for samples 1 (*a*), 2 (*b*), 3 (*c*), and 4 (*d*)

obtained showed that, regardless of the testing pattern, sample 3 had the highest wear resistance and greatest hardness H, elastic strain resistance H/E, and plastic strain resistance H^3/E^2.

Therefore, a nanocomposite with improved mechanical and tribological properties was produced by cold pressing of the 49.47Fe–31.04Cu–8.73Ni–7.76Sn–3VN mixture with 5,000–25,000 nm grains and subsequent vacuum hot pressing. High H, H/E, and H^3/E^2 parameters and a relatively low elastic modulus are indicative of high wear resistance of the sintered composite. To predict the wear resistance, the H/E and H^3/E^2 parameters characterizing the elastic strain resistance and plastic strain resistance can be used. The composition of this sample and the method and conditions of its sintering are recommended for producing diamond-containing composites for extreme friction and wear applications.

CONCLUSIONS

The mechanical and tribological properties of the Fe–Cu–Ni–Sn–VN composites produced by cold pressing and subsequent vacuum hot pressing vary with temperature. When temperature increases from 800 to 1000°C, the hardness of the Fe–Cu–Ni–Sn–VN composite increases from 3.75 to 5.37 GPa and its elastic modulus decreases from 176 to 125 GPa. The H/E and H^3/E^2 parameters describing the elastic strain resistance and plastic strain resistance increase from 0.021 to 0.043 and from 1.70 to 9.91 MPa.

The main factor that improves the mechanical properties of the composites is that the grains are refined from 5–50 μm to 20–400 nm through the $\alpha \rightarrow \gamma \rightarrow \alpha$ transformation when VN dissolves in α-Fe.

The grain refinement from 5–50 μm to 20–400 nm and the above structural factors decrease the friction force from 115 to 80 mN and the wear rate from $1.93 \cdot 10^{-5}$ to $0.45 \cdot 10^{-5}$ mm$^3 \cdot$ N$^{-1} \cdot$ m^{-1}.

The maximum friction force (~125 mN) and wear rate (~$2.46 \cdot 10^{-5}$ $mm^3 \cdot N^{-1} \cdot m^{-1}$) have been revealed for the Fe–Cu–Ni–Sn composite sintered at 800°C and subjected to additional hot pressing. This composite is characterized by coarse-grained (~5−50 μm) structure and minimum hardness (~2.68 GPa), elastic strain resistance (~0.013), and plastic strain resistance (~0.49 MPa).

Wear resistance tests, in combination with nanohardness and elastic modulus measurements, indicate that the functional capabilities of the developed composite with a nanocrystalline matrix can be expended substantially.

ACKNOWLEDGEMENTS

The research has been conducted within a state-budget research program in compliance with coordination plans of the Ministry for Education and Science of Ukraine (State Registration No. 0117U000391).

REFERENCES

1. V.A. Mechnik, “Diamond–Fe–Cu–Ni–Sn composites with predictably stable characteristics,” *Fiz. Khim. Mekh. Mater.*, No. 5, 34–42 (2012).
2. A.A. Zaitsev, D.A. Sidorenko, E.A. Levashov, V.V. Kurbatkina, S.I. Rupasov, and P.V. Sevastianov, “Development and use of a precipitation-strengthened Cu–Ni–Fe–Sn alloy matrix for hardmetal cutting tools,” *Sverkhtverd. Mater.*, No. 4, 75−88 (2012).
3. D.A. Sidorenko, A.A. Zaitsev, A.N. Kirichenko, E.A. Levashov, V.V. Kurbatkina, P.A. Loginov, S.I. Rupasov, and V.A. Andreev, “Interaction of diamond grains with nanosized alloying agents in metal–matrix composites as studied by Raman spectroscopy,” *Diamond Relat. Mater.*, No. 38, 59−62 (2013).
4. V.A. Mechnik, “Production of diamond–(Fe−Cu−Ni−Sn) composites with high wear resistance,” *Powder Metall. Met. Ceram.*, **52**, No. 9−10, 577−587 (2014).
5. V.A. Mechnik, N.A. Bondarenko, N.O. Kuzin, and B.A. Lyashenko, “Role of structurization in the mechanical properties of diamond−(Fe−Cu−Ni−Sn) composites,” *Trenie Iznos*, **37**, No. 4, 482–490 (2016).
6. Z. Nitkiewicz and M. Swierzy, “Tin influence on diamond-metal matrix hot pressed tools for stone cutting,” *J. Mater. Proc. Tech.*, **175**, No. 1–3, 306–315 (2006).
7. E. Gevorkyan, V. Mechnik, N. Bondarenko, R. Vovk, S. Lytovchenko, V. Chishkala, and O. Melnik, “Peculiarities of obtaining diamond–(Fe–Cu–Ni–Sn) composite materials by hot pressing,” *Funct. Mater.*, No. 24, 31–45 (2017).
8. Janusz Konstanty, *Powder Metallurgy Diamond Tools*, Oxford, UK (2005).
9. V.A. Aleksandrov, N.A. Alekseenko, and V.A. Mechnik, “Study of force and energy parameters in the cutting of granite with rotary diamond saws,” *Sverkhtverd. Mater.*, No. 6, 35−39 (1984).
10. A.N. Zhukovskii, A.L. Maistrenko, V.A. Mechnik, and N.A. Bondarenko, “Stress–strain state of the matrix near the diamond grains subjected to normal and tangential loads. Part 1. Model,” *Trenie Iznos*, **23**, No. 3, 146–153 (2002).
11. A.N. Zhukovskii, A.L. Maistrenko, V.A. Mechnik, and N.A. Bondarenko, “Stress–strain state of the matrix near the diamond grains subjected to normal and tangential loads. Part 2. Analysis,” *Trenie Iznos*, **23**, No. 4, 393–396 (2002).
12. V.A. Aleksandrov, A.N. Zhukovskii, and V.A. Mechnik, “Temperature field and wear of inhomogeneous diamond disk in convective heat transfer. Part 1,” *Trenie Iznos*, **15**, No. 1, 27–35 (1994).
13. V.A. Aleksandrov, A.N. Zhukovskii, and V.A. Mechnik, "Temperature field and wear of inhomogeneous diamond disk in convective heat transfer. Part 2," *Trenie Iznos*, **15**, No. 2, 196–201 (1994).
14. V.A. Dutka, V.M. Kolodnitskyi, S.D. Zabolotny, I.A. Sveshnikov, and V.A. Lukash, “Modeling the temperature level in rock cutting components of drilling bits,” *Sverkhtverd. Mater.*, No. 2, 66–73 (2004).
15. V.A. Dutka, V.M. Kolodnitskyi, O.V. Melnichuk, and S.D. Zabolotny, “Mathematical model of thermal processes in interaction of rock cutting components of drilling bits with rock masses,” *Sverkhtverd. Mater.*, No. 1, 67–77 (2005).

16. V.A. Aleksandrov and V.A. Mechnik, “Effect of the thermal conductivity of diamonds and heat exchange coefficient on the contact temperature and wear of cutting wheels,” *Trenie Iznos*, **14**, No. 6, 1115–1117 (1993).
17. V.A. Aleksandrov, A.N. Zhukovskii, and V.A. Mechnik, “Temperature field, thermoelastic state, and wear of diamond wheel in cutting with cooling. Part 1,” *Trenie Iznos*, **12**, No. 2, 210–218 (1991).
18. V.A. Aleksandrov, A.N. Zhukovskii, and V.A. Mechnik, “Temperature field, thermoelastic state, and wear of diamond wheel in cutting with cooling. Part 2,” *Trenie Iznos*, **12**, No. 3, 417–427 (1991).
19. A.A. Zaitsev, D.A. Sidorenko, E.A. Levashov, V.V. Kurbatkina, V.A. Andreev, and S.I. Rupasov, “Diamond tools for cutting highly reinforced concrete with a nanoparticle-strengthened metallic matrix,” *Sverkhtverd. Mater.*, No. 6, 78–89 (2010).
20. V.A. Mechnik, “Structurization in the diamond–Fe–Cu–Ni–Sn–CrB_2 system,” *Fiz. Khim. Mekh. Mater.*, No. 1, 85–92 (2013).
21. V.A. Mechnik, “Effect of hot recompaction parameters on the structure and properties of diamond–(Fe–Cu–Ni–Sn–CrB_2) composites,” *Powder Metall. Met. Ceram.*, **52**, No. 11–12, 709–721 (2014).
22. V.N. Kolodnitskyi and O.V. Bagirov, “On structurization of diamond-containing composites used in drilling and stone-processing tools (Overview),” *Sverkhtverd. Mater.*, No. 1, 3–26 (2017).
23. V.A. Mechnik, N.A. Bondarenko, N.O. Kuzin, and E.S. Gevorkian, “Effect of VN additions on the structure and service properties of diamond–(Fe–Cu–Ni–Sn) composites,” *Trenie Iznos*, **39**, No. 2, 101–107 (2018).
24. S. Zhang, X. L. Bui, J. Jiang, and X. Li, “Microstructure and tribological properties of magnetron sputtered nc-TiC/a-C nanocomposites,” *Surf. Coat. Technol*., **198**, 206–211 (2005).
25. B.K. Tay, Y.H. Cheng, X.Z. Ding, S.P. Lau, X. Shi, G.F. You, and D. Sheeja, “Hard carbon nanocomposite films with low stress,” *Diamond Relat. Mater.*, **10**, 1082–1087 (2001).
26. D.G. Teer, “New solid lubricant coatings,” *Wear*, **251**, 1068–1074 (2001).
27. Z.Z. Valiev and I.V. Aleksandrov, *Bulk Nanostructured Materials* [in Russian], IKTs Akademkniga, Moscow (2007).
28. Yu.I. Golovin, *Introduction to Nanoengineering* [in Russian], Mashinostroenie, Moscow (2007).
29. J. Musil, “Tribological and mechanical properties of nanocrystalline n-TiC/a-C nanocomposite thin films,” *J. Vac. Sci. Technol. A*, **28**, No. 2, 244–249 (2010).
30. H. Gleiter, “Nanostructured materials: basic concepts and microstructure,” *Acta Mater*., **48**, 1–29 (2000).
31. H. Gleiter, “Materials with ultrafine microstructures: Retrospectives and perspectives,” *Nanostruct. Mater.*, No. 1, 1–19 (1992).
32. A.I. Gusev, *Nanomaterials, Nanostructures, and Nanotechnologies* [in Russian], Fizmatlit, Moscow (2009), p. 416.
33. W.U. Zhiwei, J. Zhang, Yi Chen, and M. Liang, “Effect of rare earth addition on microstructural, mechanical and electrical characteristics of Cu–6% Fe microcomposites,” *J. Rare Earths*, **27**, No. 1, 87–91 (2009).
34. L. He and E. Ma, “Processing and microhardness of bulk Cu–Fe,” *Nanostruct. Mater.*, **7**, No. 3, 327–339 (1996).
35. N.A. Akhmadeev, N.P. Kobelev, R.R. Mulyukov, Ya.M. Soifer, and R.Z. Valiev, “The effect of heat treatment on the elastic and dissipative properties of copper with the submicrocrystalline structure,” *Acta Metall. Mater*., **41**, No. 4, 1041–1046 (1993).
36. A.I. Gusev, “Effects of the nanocrystalline state in solids,” *Fiz. Usp.*, **41**, 49–76 (1998).
37. A. Robertson, U. Erb, and G. Palumbo, “Practical applications for electrodeposited nanocrystalline materials,” *Nanostruct. Mater.*, **12**, No. 5–8, 1035–1040 (1999).
38. V.A. Mechnik, N.A. Bondarenko, S.N. Dub, V.M. Kolodnitskyi, Yu.V. Nesterenko, N.O. Kuzin, I.M. Zakiev, and E.S. Gevorkyan, “A study of microstructure of Fe–Cu–Ni–Sn and Fe–Cu–Ni–Sn–VN metal matrix for diamond containing composites,” *Mater. Charact.*, **146**, 209–216 (2018).

39. V.A. Mechnik, N.A. Bondarenko, V.M. Kolodnitskyi, V.I. Zakiev, I.M. Zakiev, M. Storchak, S.N. Dub, and N.O. Kuzin, “Physico-mechanical and tribological properties of Fe–Cu–Ni–Sn and Fe–Cu–Ni–Sn–VN nanocomposites obtained by powder metallurgy methods,” *Tribol. Ind*., **41**, No. 2, 188–198 (2019).
40. E. Rabinowicz, *Friction and Wear of Materials*, Wiley, New York (1995).
41. A. Leyland and A. Matthews, “On the significance of the *H*/*E* ratio in wear control: a nanocomposite coating approach to optimized tribological behavior,” *Wear*, No. 246, 1–11 (2000).
42. N.V. Novikov, M.A. Voronkin, S.N. Dub, I.N. Lupich, V.G. Malogolovets, B.A. Maslyuk, and G.A. Podzyarey, “Transition from polymer-like to diamond-like a-C:H films: Structure and mechanical properties,” *Diamond Related. Mater.*, No. 6, 574–578 (1997).
43. J. Soldan and J. Musil, “Structure and mechanical properties of DC magnetron sputtered TiC/Cu films,” *Vacuum*, No. 81, 531–538 (2006).
44. J. Musil, “Tribological and mechanical properties of nanocrystalline n-TiC/a-C nanocomposites thin films,” *J. Vac. Sci. Technol. A*, **28**, No. 2, 244–249 (2010).
45. I.A. Sveshnikov and V.N. Kolodnitskyi, “Optimization of placing hardmetal cutters in drill bits,” *Sverkhtverd. Mater.*, No. 4, 70–75 (2006).
46. V.Y. Kodash and E.S. Gevorkian, “Tungsten carbide cutting tool materials,” *US Patent 6617271 B1*, IC C04B 35/56, publ. September 9 (2003).
47. W. Kraus and G. Nolze, “Powder Cell–A program for the representation and manipulation of crystal structures and calculation of the resulting X-ray powder patterns,” *J. Appl. Crystallogr.*, No. 29, 301–303 (1996).
48. *Selected Powder Diffraction Data for Education Straining (Search Manual and Data Cards)*, International Centre for Diffraction Data, USA (1988), p. 432.
49. W. C. Oliver and G. M. Pharr, “An improved technique for determining hardness and elastic modulus using load and displacement sensing indentation experiments,” *J. Mater. Res.*, **7**, 1564–1583 (1992).
50. V. Zakiev, A. Markovsky, E. Aznakayev, I. Zakiev, and E. Gursky, “Micro-mechanical properties of bio-materials,” in: *Proc. SPIE 5959, Medical Imaging, 595916* (September 23, 2005), Event: Congress on Optics and Optoelectronics, Warsaw, Poland (2005), doi:10.1117/12.628396
51. S.A. Firstov, V.F. Gorban, N.A. Krapivka, E.P. Pechkovskii, N.I. Danilenko, and M.V. Karpets, “Mechanical properties of multicomponent titanium alloy,” *Strength Mater.*, No. 42, 622–630 (2010).
52. Y.L. Hao, S.J. Li, S.Y. Sun, C.Y. Zheng, and R. Vang, “Elastic deformation behavior of Ti–24Nb–4Zn–7.9Sn for biomedical application,” *Acta Biomater.*, **3**, No. 2, 277–286 (2007).
53. S. Hassani, M. Bielawski, W. Beres, L. Martinu, M. Balazinski, and J.E. Klemberg-Sapieha, “Predictive tools for the design of erosion resistant coatings,” *Surf. Coat. Technol*., **203**, 204–210 (2008).
54. E. Bousser, M. Benkahoul, L. Martinu, and J.E. Klemberg-Sapieha, “Effect of microstructure on the erosion resistance of Cr–Si–N coatings,” *Surf. Coat. Technol*., **203**, 776–778 (2008).